INTERNATIONAL JOURNAL FOR NUMERICAL METHODS IN FLUIDS
Int. J. Numer. Meth. Fluids 2009; **00**:1–26 *Prepared using* fldauth.cls *[Version: 2002/09/18 v1.01]*

Using Adjoint Error Estimation Techniques for Elastohydrodynamic Lubrication Line Contact Problems

D.E. Hart[1], M. Berzins[2,], C.E. Goodyer[1*], P.K. Jimack[1]

[1] *School of Computing, University of Leeds, Leeds, LS2 9JT, United Kingdom*
[2] *School of Computing, University of Utah, Salt Lake City, Utah, USA*

SUMMARY

The use of an adjoint technique for goal-based error estimation described by Hart *et al.* (this journal, volume 47, pages 1069–1074) is extended to the numerical solution of free boundary problems that arise in elastohydrodynamic lubrication (EHL). EHL systems are highly nonlinear and consist of a thin-film approximation of the flow of a non-Newtonian lubricant which separates two bodies that are forced together by an applied load, coupled with a linear elastic model for the deformation of the bodies. A finite difference discretization of the line contact flow problem is presented, along with the numerical evaluation of an exact solution for the elastic deformation, and a moving grid representation of the free boundary that models cavitation at the outflow in this one dimensional case. The application of a goal-based error estimate for this problem is then described. This estimate relies on the solution of an adjoint problem; its effectiveness is demonstrated for the physically important goal of the total friction through the contact. Finally, the application of this error estimate to drive local mesh refinement is demonstrated. Copyright © 2009 John Wiley & Sons, Ltd.

KEY WORDS: Elastohydrodynamic lubrication, Goal-based error estimates, Discrete adjoints, Friction

1. Introduction

Elastohydrodynamic lubrication (EHL) describes the flow of a lubricating fluid which separates two solid bodies that are being forced together by a large external load. In particular, EHL represents the case where this load, and the resulting pressures in the fluid, are sufficiently high as to lead the solid bodies to deform. The purpose of separating the bodies with a thin lubricating film is to reduce the friction in the contact, thus increasing the efficiency of energy transfer through the contact, and reducing the wear on the contacting elements. Consequently, when modelling an EHL contact numerically, whilst flow field properties such as the pressure distribution or the thickness of the film are significant, it is often quantities such as the friction, that are of most interest, [5, 6].

The purpose of this paper is to demonstrate how goal-based error estimates may be developed that specifically target derived quantities such as friction, in order to provide reliable information on the accuracy of such EHL solutions, and to guide local mesh refinement for these problems. Our approach is to build upon an earlier, exploratory study, [10], which applied the techniques used here

*Correspondence to: c.e.goodyer@leeds.ac.uk

(based upon [18–20]) to a simple model problem. The contribution of this paper is to show that this methodology can be extended successfully to the full EHL problem with a realistic model of film thickness and the application of adaptive meshes.

Solution times for numerical models of EHL problems continue to decrease as the algorithms used improve and the computers on which they are solved become more powerful. For example as with the authors' *Carmehl* software that is used by Shell, [8], EHL solvers are used by industry within optimisation processes to match known experimental calculations of friction across a wide range of operating conditions in order to estimate the many model parameters that describe the lubricant. This leads to thousands of different computational cases, all of which need very accurate calculations of the friction. Furthermore, as the lubricant used by industry become more complex, the demands for robustness, accuracy and speed of the software continue to increase. Often research into error estimation and control has tended to assume that it is the overall accuracy of the computed solution which is of interest. In many practical situations however, the solution field is used to calculate some derived quantity, such as friction, drag, lift, etc, [18–20].

Investigations into friction have been mainly confined to experimental work such as Blencoe *et al.* [3] and Workel *et al.* [21]. An important feature of typical EHL solutions is a clearly defined spike in the pressure field near the outflow of the contact region, and estimating the friction reliably appears to be closely related to accurately capturing the profile of this pressure spike. Work by Bisset and Glander [1] showed that when more mesh points are used in the region of the spike then it is no longer seen as a singularity in the solution, but a smooth profile. This work only resolved the spike using up to 1000 points, however it did still highlight the importance of this area of the solution. More recent results in [7, 11] used over a million mesh points and illustrated both the smoothness of the pressure spike and the need for appropriate levels of mesh refinement. Consequently, calculating the friction accurately depends on achieving the necessary resolution of the pressure profile.

The approach taken here to estimate the error in the computed friction is to make use of adjoint methods to calculate the sensitivity of the output quantity of interest to other computable quantities. This involves formulating and solving an adjoint system from the original "forward" problem. There are two distinct but related approaches to formulating such a system: continuous and discrete, see Nadarajah and Jameson [14]. The approach followed here is that developed by Darmofal and Venditti [18–20]. This is a discrete adjoint formulation which, as stated in [19], "is a discrete analogue of the Pierce and Giles [15] technique". The main reasons for our choice of this method over the approach of [15] is that, for a complex EHL problem, formulating the continuous adjoint problem (including appropriate boundary conditions) would be non-trivial. Through the use of the discrete approach however, adjoint error estimation becomes a realistic prospect for application to EHL.

2. Governing equations and their discretization

The governing equations for EHL are based upon a long-wave approximation to the flow in the contact, which simplifies the Navier-Stokes equations by assuming that inertial terms and the variation in the normal direction are both negligible, coupled with a small elastic deformation for the contacting elements. The former approximation leads to the Reynolds equation (see below) whilst the latter leads to an analytic solution which requires the evaluation of a line integral (also shown below). Additional features of the model include a force balance constraint and a free boundary condition, which represents the fact that the model is only valid for positive pressures yet the location at which the pressure becomes negative (the cavitation position) is unknown *a priori*.

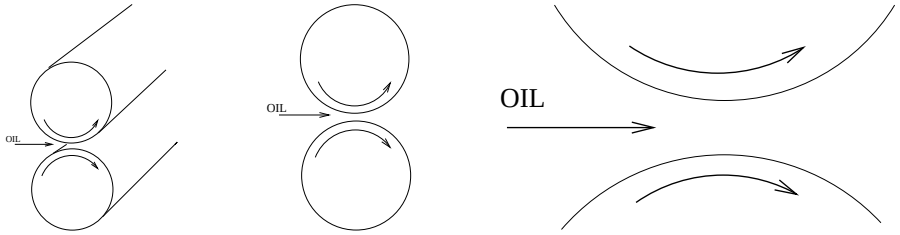

Figure 1. Illustration of an idealized line contact.

For this work we consider line contact problems in which two cylinders are aligned with their axes of rotation parallel and are in close contact separated by a lubricating film. Such a case is illustrated in Figure 1 and provides an idealised model for numerous common interactions. By ignoring end effects, it is only necessary to model the behaviour at a single cross-section of the line contact with a single independent variable, which represents the distance across the contact. All of the equations presented are the standard non-dimensionalized form [9].

2.1. Elastohydrodynamic lubrication line contact

The Reynolds equation for the full line contact is given by

$$\frac{\partial}{\partial X}\left(\varepsilon\frac{\partial P}{\partial X}\right)-\frac{\partial(\overline{\rho}H)}{\partial X}=0, \tag{1}$$

with the film thickness equation, based upon the linear elastic assumption, given by

$$H=H_0+\frac{X^2}{2}+\frac{1}{\pi}\int_{-\infty}^{\infty}\ln|X-X'|P(X')\mathrm{d}X'. \tag{2}$$

In these equations $P(X)$ is the pressure field, $H(X)$ is the film thickness field, H_0 is the central offset distance, $\overline{\rho}(X)$ is the density (see (3) below) and $\varepsilon=\frac{H^3\overline{\rho}}{\lambda\overline{\eta}}$, where λ is a known constant (depending upon the relative motion of the contacting elements) and $\overline{\eta}(X)$ is the viscosity. For this work we make use of the viscosity and density models of [16] and [4] respectively:

$$\overline{\eta}=\exp\left\{\left(\frac{\alpha p_0}{z}\right)\left(-1+\left[1+\frac{Pp_h}{p_0}\right]^z\right)\right\}\quad\text{and}\quad\overline{\rho}=\frac{0.59\times10^9+1.34Pp_h}{0.59\times10^9+Pp_h}. \tag{3}$$

In each of these expressions p_h is the representative pressure that has been used in the non-dimensionalization of the equations. The examples in the rest of this paper use the parameters λ=60.7, α=1.43$\times10^{-8}$, p_0=1.96$\times10^8$ and z=0.68. Finally, we state the force-balance equation which requires that the sum of the pressure is equal to the applied load:

$$\int_{-\infty}^{\infty}P\,\mathrm{d}X=\frac{\pi}{2}. \tag{4}$$

In equations (1) to (4) it is possible to treat just $P(X)$ and H_0 as unknowns since, once these have been found, all of the other quantities may be determined. A further unknown must also be introduced however, to capture the position of the free boundary, at which cavitation occurs. We will denote this position as X_c, which must be found such that the boundary condition

$$P'(X_c)=0 \tag{5}$$

holds, reflecting the fact that the pressure should not be allowed to go negative. If we also approximate the domain by a finite interval of length D and impose zero Dirichlet boundary conditions for pressure, then we must also satisfy

$$P(X_c - D) = P(X_c) = 0\,. \tag{6}$$

2.2. Friction

Friction is a force which opposes motion and in an EHL contact is given by the shear stress generated within the lubricant. This comes about through two mechanisms, rolling friction and kinetic (sliding) friction. Within the contact, a pressure gradient is generated. This is because the deformation of the contact is largest in the centre, requiring the greatest pressure to maintain it. As the two surfaces move through the contact, lubricant is pulled with them (entrained). However, it is also squeezed out by the pressure generated in the contact region, and so the lubricant in the middle is moving at a different speed to the surfaces, causing it to shear. The resistance to this motion is called the rolling friction and forms the first term of each expression in (7) below. The second mechanism for the generation of shear stress only happens when the surfaces are in relative motion, hence sliding friction. Now, the lubricant is sheared at the rate of the difference in speed of the two surfaces per unit thickness. It is therefore possible to derive the shear stress on each surface [17]:

$$\tau_{xz;a}(x) = -\frac{h}{2}\frac{\partial p}{\partial x} + \frac{\eta}{h}(u_b - u_a) \quad \text{and} \quad \tau_{xz;b}(x) = \frac{h}{2}\frac{\partial p}{\partial x} + \frac{\eta}{h}(u_b - u_a)\,, \tag{7}$$

for the lower and upper surfaces moving at speeds u_a and u_b respectively. Note that, following [17], we express (7) in dimensional form here. Hence, from these expressions, it is possible to work out the total dimensional friction through a line contact, F as either

$$F = \int_{-\infty}^{\infty} \tau_{xz;a}(x)\mathrm{d}x \quad \text{or} \quad F = \int_{-\infty}^{\infty} -\tau_{xz;b}(x)\mathrm{d}x\,, \tag{8}$$

depending on which surface is required. In this work, the friction on the lower surface will be used, i.e. the first equality in equation (8), although this choice is arbitrary. This is a key quantity of interest as it gives a measure of the force opposing the shear in the lubricant, e.g. [2].

2.3. Discretization

In discretizing equations (1) to (6) the computational domain, $X_c - D \leqslant X \leqslant X_c$, is divided into $n-1$ intervals, to form a grid with n nodes located at points $X_i = X_c - D + i\Delta X$, for $i = 0,\ldots,n-1$, where $\Delta X = D/(n-1)$. This assumption of equally spaced nodes is made here primarily to simplify the exposition in this section, the straightforward extension to non-uniform grids being used for the local mesh refinement results presented below. As indicated in Section 2.1, the primary unknowns for the EHL problem are $P(X)$, H_0 and X_c and are represented by the $n+2$ unknowns: $P_0,\ldots,P_{n-1}$, H_0 and X_c. In order to determine these unknowns, a system of $n+2$ nonlinear equations is defined, based upon the discretization of equations (1) to (6). These may be represented as the residual equations: $R_i = 0$ ($i = 0,\ldots,n-1$), $R_{X_c} = 0$ and $R_{H_0} = 0$. The Dirichlet boundary conditions (6) allow the residuals for the two end points of the domain to be given simply by

$$R_0 = -P_0 \qquad \text{and} \qquad R_{n-1} = -P_{n-1}\,. \tag{9}$$

Application of a standard finite difference scheme to the Reynolds equation (1) yields the next $n-2$ of the residual expressions, for points $i = 1 \ldots n-2$:

$$\begin{aligned} R_i &= \Delta X \left(\left(\frac{\overline{\rho}_i H_i - \overline{\rho}_{i-1} H_{i-1}}{\Delta X} \right) - \left(\frac{(P_{i+1} - P_i)\varepsilon_{i+\frac{1}{2}} - (P_i - P_{i-1})\varepsilon_{i-\frac{1}{2}}}{(\Delta X)^2} \right) \right) \\ &= \left(\overline{\rho}_i H_i - \overline{\rho}_{i-1} H_{i-1}\right) - \left(\frac{(P_{i+1} - P_i)\varepsilon_{i+\frac{1}{2}} - (P_i - P_{i-1})\varepsilon_{i-\frac{1}{2}}}{\Delta X} \right) \qquad (10) \\ &= \left(\overline{\rho}_i H_i - \overline{\rho}_{i-1} H_{i-1}\right) - \left(\frac{\varepsilon_{i+\frac{1}{2}} P_{i+1} - (\varepsilon_{i+\frac{1}{2}} + \varepsilon_{i-\frac{1}{2}}) P_i + \varepsilon_{i-\frac{1}{2}} P_{i-1}}{\Delta X} \right), \qquad (11) \end{aligned}$$

where $\varepsilon_i = \frac{H_i^3 \overline{\rho}_i}{\lambda \overline{\eta}_i}$, $\varepsilon_{i\pm\frac{1}{2}} = (\varepsilon_i + \varepsilon_{i\pm1})/2$, and the discrete form of H_i, $\overline{\eta}_i$, and $\overline{\rho}_i$ are given respectively by

$$H_i = H_0 + \frac{X_i^2}{2} + \frac{1}{\pi} \sum_{j=0}^{n-1} K_{ij} P_j, \qquad (12)$$

$$\overline{\eta}_i = \exp\left\{ \left(\frac{\alpha p_0}{z} \right) \left(-1 + \left[1 + \frac{P_i p_h}{p_0} \right]^z \right) \right\} \quad \text{and} \quad \overline{\rho}_i = \frac{0.59 \times 10^9 + 1.34 P_i p_h}{0.59 \times 10^9 + P_i p_h}, \qquad (13)$$

the matrix K in (12) depending upon the quadrature rule that is selected for the evaluation of (2). In this work the following standard equation is used:

$$K_{ij} = \left(i - j + \tfrac{1}{2}\right) \Delta X \left(\ln\left(\left| i - j + \tfrac{1}{2} \right| \Delta X \right) - 1 \right) - \left(i - j - \tfrac{1}{2}\right) \Delta X \left(\ln\left| i - j - \tfrac{1}{2} \right| \Delta X - 1 \right). \qquad (14)$$

The residual equation from discretizing equation (4) is expressed as

$$R_{H_0} = \frac{\pi}{2} - \sum_{i=0}^{n-2} \frac{P_i + P_{i+1}}{2} \Delta X, \qquad (15)$$

whilst discretization of (5) is gained through the second order upwind finite difference approximation, $P'(X_i) \approx \frac{3P_i - 4P_{i-1} + P_{i-2}}{2\Delta X}$. By evaluating this at the boundary point $i = n-1$, and noting that $P_{n-1} = 0$, this residual can be expressed as

$$R_{X_c} = -\frac{4P_{n-2} - P_{n-3}}{2\Delta X}. \qquad (16)$$

This scheme, involving a first order upwind discretization term in the Reynolds equation, is typical for stable finite difference and low-order finite element discretizations. Recently, higher order alternatives have been proposed, e.g. [12], however these have yet to be widely used in practice.

2.4. Solution of the discrete system

In solving equations (9), (11), (15) and (16), our goal is to obtain a simple and robust algorithm which will allow our error estimates to be assessed and so we do not focus on matters associated with tuning the speed and efficiency of the solver in this section. Although the system could be solved with a black-box quasi-Newton nonlinear solver, this is not as robust for EHL problems as using the nested iteration described here. Hence we use a nested iteration based upon a nonlinear solver for equations (9), (11) and (15), coupled together using *Carmehl*, [8], as the inner part of the nest. Outside this, another iteration is used to update X_c as shown:

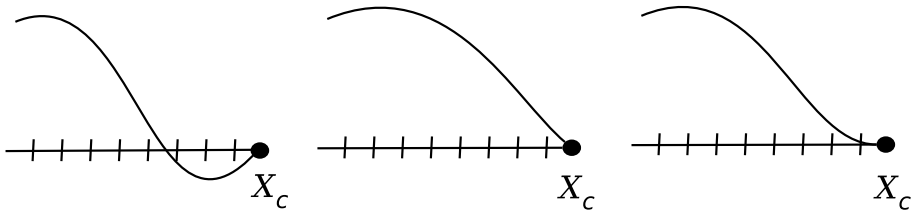

(a) $P'(X_c) > 0$ (b) $P'(X_c) < 0$ (c) $P'(X_c) = 0$

Figure 2. The three cases for the right-hand boundary. When deciding how to move this boundary position, cases (a) and (b) result in the mesh moving either left or right respectively.

0. Provide an initial guess for H_0, X_c and $P_0, ..., P_{n-1}$.
1. Solve the nonlinear system (9), (11) and (15) for $P_0, ..., P_{n-1}$ and H_0.
2. Find the correct X_c for the current P_{n-3} and P_{n-2} (using (16)).
3. If X_c has not converged go to step 1.

The initial guess used for the nonlinear solver in step 1 is based upon the previous solution that has been obtained; with the very initial guess coming from step 0. Given a solution for P and H_0 from step 1, the cavitation boundary position may be updated so as to satisfy (16). For the latest value of X_c, if the gradient of P is sufficiently close to zero (i.e. $\left|\frac{-4P_{n-2}+P_{n-3}}{2\Delta X}\right| < 10^{-8}$, say), then cavitation point X_c has been found and the algorithm is complete. If not then X_c is updated by repeated use of the bisection algorithm. Figure 2, case (a), shows that the gradient is positive at X_c, and the boundary is too far to the right (so X_c should be decreased); in case (b), the gradient is negative at X_c, and the boundary is too far left (so X_c should be increased). An initial bracket is easily obtained based upon the sign of the slope at the initial X_c and then selecting a sufficiently large or small value to obtain $P'(X_c)$ with the opposite sign. Figure 2(c) shows a converged solution with $P'(X_c) = 0$. Note that each time X_c is updated it is necessary to return to step 1 in order to update P and H_0.

2.5. Typical line contact solutions

An important, and typical, feature of EHL line contact solutions is the "spike" that appears in the pressure field towards the outflow region of the contact. (Examples of this, for different applied loads, are clearly visible in the pressure solutions given in Figure 4, below, for example.) An illustration of the level of mesh resolution that is required to capture this pressure spike very accurately is provided in [7], where the mesh density is repeatedly doubled and the resulting changes in the pressure solution, and also in the derived friction, are observed. As the mesh is refined the pressure profiles are almost coincidental apart from around the pressure spike, however the computed friction is not identical in each case. This change in the friction is illustrated in Table I, along with specific features of the pressure (its maximum value at the spike) and the film thickness (its minimum value). It is the derivatives of pressure in equations (7) and (8) that are especially important in friction calculations. If the pressure spike is not captured well enough then these derivatives will not represent the true friction through the contact. Figure 3 illustrates convergence of the shear stress with uniform mesh refinement: it is clear from this figure and Table I that grid levels for which quantities such as film thickness appear to have converged are still not sufficiently fine to capture the shear stress to the same accuracy.

Mesh Level	8	9	10	11	12	13
Spike Height	0.816	0.827	0.857	0.891	0.919	0.938
Min. Film Thickness	0.1458	0.1443	0.1429	0.1420	0.1415	0.1413
Friction ($\times 10^{-4}$)	9.485	9.066	8.889	8.797	8.749	8.718

Mesh Level	14	15	16	17	18	19
Spike Height	0.951	0.958	0.961	0.963	0.964	0.965
Min Film Thickness	0.1411	0.1410	0.1410	0.1410	0.1410	0.1410
Friction ($\times 10^{-4}$)	8.700	8.690	8.685	8.682	8.681	8.680

Table I. Value of Pressure Spike Height, Minimum Film Thickness and Friction for mesh level i corresponding to $2^i + 1$ points.

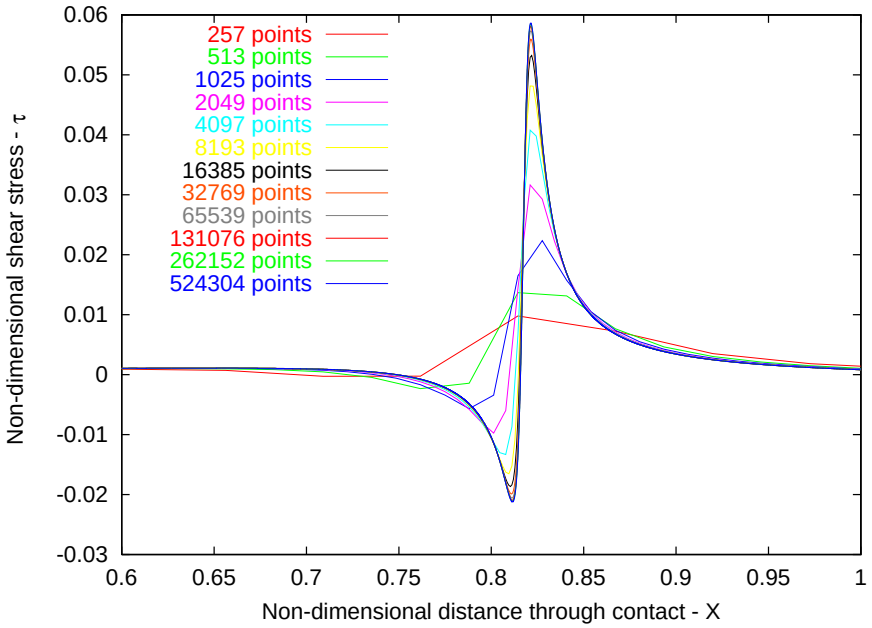

Figure 3. Shear stress profiles with increasing grid resolution for a line contact case.

3. Adjoint error estimation

This section describes the goal-based error estimation procedure that we apply to the line contact EHL problem outlined above. The descriptions provided are deliberately very general, so as to illustrate the full versatility of the approach. However, [9] illustrates some of the specific implementation details for the discrete adjoint of the system of equations given in Section 2.3.

3.1. Adjoint formulation

This formulation is that of Vendetti and Darmofal [18–20]. Their starting point is to define two meshes with spacing $h = \Delta x$ and $H = \Delta X = m \times \Delta x$, $\{m \in \mathbb{N} \mid m > 1\}$ (i.e. H is some multiple of the mesh

space size h). The idea is that mesh size H is fine enough to capture the features of the problem being solved, and coarse enough to be solved in a reasonable time, while the fine mesh size h would give the solution to a greater accuracy but in an unacceptable time. Whilst the coarser of the two meshes need not necessarily be very coarse, nor necessarily the finer mesh particularly fine, for ease of terminology these two meshes will be referred to as the coarse mesh and the fine mesh hereafter.

Consider an arbitrary nonlinear problem whose discrete form may be represented as $A_h(u_h) = f_h$ on the fine mesh and $A_H(u_H) = f_H$ on the coarse mesh, where in each case $A(u)$ is a nonlinear operator. Let u_h^H be an approximation to u_h obtained by interpolation of the coarse mesh solution: $u_h^H = I_h^H u_H$. Throughout this paper the solution u will be referred to as the forward solution and the interpolation for both the forward and the adjoint solution will be through cubic splines. The discrete fine grid and coarse grid residuals are given by

$$R_h(u_h) = f_h - A_h(u_h) \quad \text{and} \quad R_H(u_H) = f_H - A_H(u_H)$$

respectively. The approach used is described in detail in [18], the goal being to estimate a quantity of interest $F_h(u_h)$ but only using information computed on the coarse mesh. To avoid repetition of the argument presented in [18], we simply note the conclusion that the following estimate may be used:

$$F_h(u_h) \approx \tilde{F}_h(u_H) = F_h(u_h^H) - (\Psi_h^H)^T R_h(u_h^H). \tag{17}$$

Here $\Psi_h^H = I_h^H \Psi_H$, where the adjoint variable Ψ_H satisfies the linear equation

$$\left[\frac{\partial R_H}{\partial u_H}\right]^T \Psi_H = \left(\frac{\partial F_H}{\partial u_H}\right)^T \tag{18}$$

on the coarse grid. An approximation to the fine grid functional has therefore been obtained simply by solving a linear adjoint problem on the coarse grid, in addition to solving the primary problem on the coarse grid. The expression $(\Psi_h^H)^T R_h(u_h^H)$ in (17) will be referred to as the "correction" to the functional $F_h(u_h^H)$. A final important point is that, as noted by in [19], "A typical finite difference stencil would need to be scaled by an appropriate volume term (or an area term in two dimensions) so that the residual became analogous to an integral expression". This has been done for equation (11) and is also key in applying the procedure correctly with non-uniform finite difference meshes, see Section 4.2.

3.2. Using adjoint-based error estimates to control grid adaptation

The *a posteriori* technique outlined in the previous subsection allows estimates of the error in the quantity of interest to be made at a relatively modest additional cost and may then be used to decide whether or not this quantity is sufficiently accurate. In the case where the error is unacceptable further refinement of the mesh may be undertaken and the solution and error estimation steps repeated on the new grid.

Using global mesh refinement involves doubling the mesh density everywhere to yield a new discrete problem with approximately twice the number of degrees of freedom. The error estimates may be used to improve the computed quantity of interest on each of these meshes. This is an accurate and robust, if expensive, procedure as uniform mesh refinement is not efficient in those regions of the domain that do not contribute greatly to the error in the quantity of interest. Local mesh refinement algorithms can be more efficient but lead to a sequence of non-uniform meshes, which requires minor modifications to the discretization and error estimation algorithms described above. Such modifications are relatively straightforward, see [9]. Note that the one place where particular care does need to be taken is in

the evaluation of the film thickness, given by (2) and approximated by (12), so as to ensure that the non-uniform mesh is accounted for appropriately, [9].

Results below show that the reliability of the error estimates are maintained in the case of non-uniform meshes, however it should be noted that the error estimate in the total friction is just a single number. In order to determine which regions of the domain should be locally refined requires estimating where the computed error is most sensitive to local mesh refinement. Here we follow the usual practice of using the regions with the greatest contribution to the error as a surrogate for this. That is, we compute $(\Psi_h^H)_i \times (R_h(u_h^H))_i$ at point i, [19], locally. The local adaptation results in the following section are based upon comparing this quantity with a prescribed refinement tolerance, as described in the following algorithm.

1. Solve forward and adjoint problems on the current non-uniform mesh (the coarse mesh).
2. Interpolate solutions onto a uniformly refined version of the coarse mesh (the fine mesh) and evaluate residuals.
3. Calculate the error correction value, defined as the last term of equation (17)
4. Define an error correction vector $\underline{v}$, such that $v_i = r_i.a_i$, where r_i is the residual and a_i is the adjoint solution at mesh point i.
5. Refine the coarse mesh where the corresponding entries of $\underline{v}$ are above a prescribed tolerance (10^{-6}).
6. Add additional refinement immediately next to refined regions ("safety layers"), in any short unrefined areas and also to ensure graded changes in the refinement level.
7. Use the interpolated solution as continuation input to the next iteration.
8. Return to step 1 if error is still too large.

This algorithm provides a means of identifying which part of the current solution contributes the most to the error in the functional of interest.

4. Computational results

In this section we assess the performance of this error estimate, and the corresponding approaches to mesh refinement, on a number of EHL test problems. Reference [9] provides specific details of the application of the adjoint method to these EHL equations along with further examples.

4.1. Uniform mesh results

Results have been computed for five different loadings, L, and a sliding case for which there is relative motion between the contacting elements ($u_a = 0.1$ and $u_b = 0.9$). The non-dimensional solution profiles for pressure are shown in Figure 4. These results were calculated using a uniform mesh of 257 points and the solutions range from being almost entirely hydrodynamic through to a relatively highly loaded EHL. Figure 4 clearly illustrates the pressure spike moving towards the outlet with increasing load, with the main pressure bump becoming increasingly rounded. The non-dimensional viscosity therefore increases dramatically with load, as a result of the exponential term in the first equation of (3).

Based upon equations (7) and (8) the dimensional friction may be seen to take the form

$$\overline{F} = \int_{-\infty}^{\infty} \left(-m_1 \frac{\partial P}{\partial X} \frac{H}{2} + m_2 \frac{\overline{\eta}}{H} (u_b - u_a) \right) \mathrm{d}X, \tag{19}$$

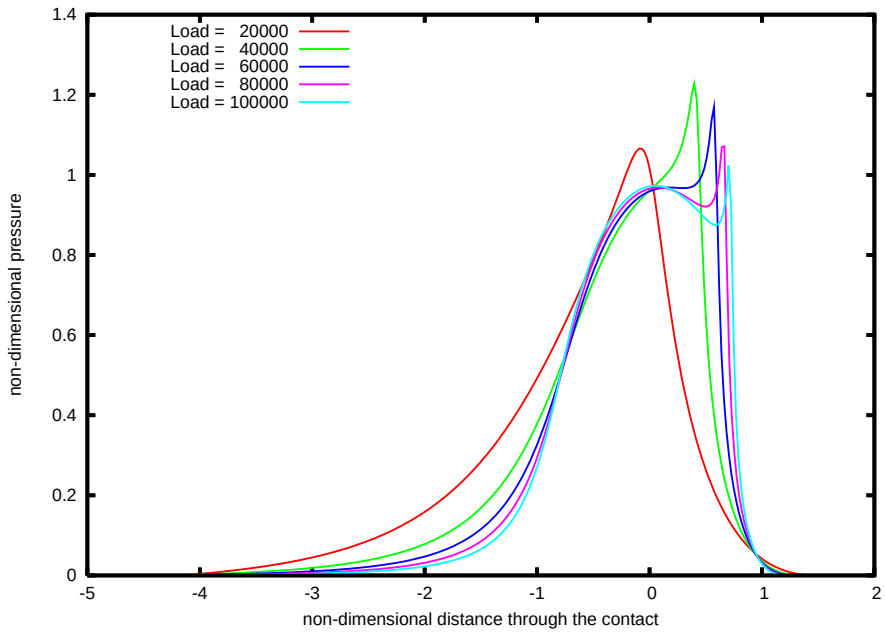

Figure 4. EHL pressure profiles for a series of loadings; $L = 20000$, 40000, 60000, 80000 and 100000.

Grid (g)	Interpolated Fric. (g)	Calculated correction	Corrected Fric. (g)	Friction ($g+1$)	Measured Error	Effectiv. Index	| 1.0 - effct. |
5	75942.4	1514.1	74428.4	74961.6	980.8	0.6478	0.3522
6	74829.4	-1429.8	76259.1	75076.2	-246.8	0.1726	0.8274
7	75062.3	-447.5	75509.9	76036.2	-973.9	2.1760	1.1760
8	76005.0	-884.2	76889.2	76898.7	-893.7	1.0108	0.0108
9	76888.4	-662.5	77550.9	77645.7	-757.4	1.1431	0.1432
10	77643.2	-468.4	78111.6	78188.4	-545.2	1.1639	0.1639
11	78187.9	-309.4	78497.2	78529.4	-341.5	1.1039	0.1039
12	78529.3	-182.7	78711.9	78722.3	-193.0	1.0567	0.0567

Table II. Adjoint based inter-grid friction error on uniform meshes; $L = 100000$, $u_a = 0.1$, $u_b = 0.9$, slide-roll ratio = 0.8 (sliding).

where the re-dimensionalizing factors m_1 and m_2 are known constants (dependent upon values used for the non-dimensionalization), see [9]. In the case considered here the non-dimensional surface speeds are $u_a = 0.1$ and $u_b = 0.9$. Figure 5 shows the adjoint solutions for the same five loads, demonstrating that there is significant activity in and around the pressure spike region. Table II shows the quality of the error estimate for the heaviest loaded (and the most challenging) case. We see that once the mesh becomes sufficiently refined the inter-grid error estimates are very good, as indicated by the convergence of the effectivity index (the ratio of the calculated correction to the measured error once the solution is found on the next mesh) to one. The error estimates are even better for the more lightly loaded cases, [9].

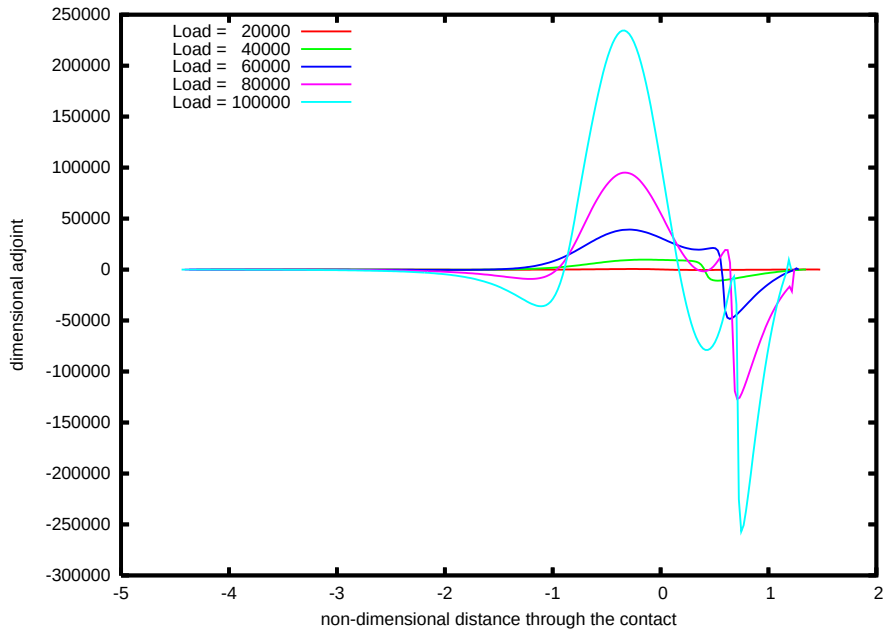

Figure 5. Adjoint solutions for EHL cases with sliding; $L = 20000$, 40000, 60000, 80000 and 100000, $u_a = 0.1$, $u_b = 0.9$.

4.2. Non-uniform mesh results

Having demonstrated the accuracy and robustness of the goal-based error estimator across a range of loading cases, we now consider the use of such an estimate to drive adaptive refinement. A different illustrative example is presented, again as representative of the full set of successful results that we have obtained. The friction is in the same form as (19), with a pure rolling considered on this occasion, with values $u_a = u_b = 0.5$ and $m_1 = 2$. Since $u_a = u_b$ then the term involving m_2 is zero.

The adaptive strategy described in subsection 3.2 is adopted. The specific regions in which refinement occurs are those for which $\left|(\Psi_h^H)_i \times (R_h(u_h^H))_i\right|$ are the greatest: where the subscript i runs through all nodes in a temporary grid (denoted with index h) which is a uniform refinement of the current computational grid (denoted with index H). In order to assess the effectiveness of this strategy, compared to solutions obtained on a sequence of uniform, globally refined grids, the error is computed by comparison against a numerical solution obtained on an excessively fine mesh is shown in Figure 6. The top line on the graph shows the error in the friction for a series of uniform grid solutions. The bottom line shows the resulting error using local adaptivity based upon the adjoint correction procedure applied to the coarse grid solution. Once the solution has been obtained on the coarse grid, it is interpolated onto a uniformly refined version, where an estimate of the friction is calculated, as if it had been computed on that fine grid. The values shown in this second graph are these adjoint-corrected estimates. The middle graph shows the equivalent corrected friction estimates when uniform refinement is used. Initially the error in the adaptive scheme is reduced in line with the uniform refinement solutions because only global refinement takes place at this stage. As the mesh is further refined, the contribution to the error is primarily found to be in certain regions, consequently

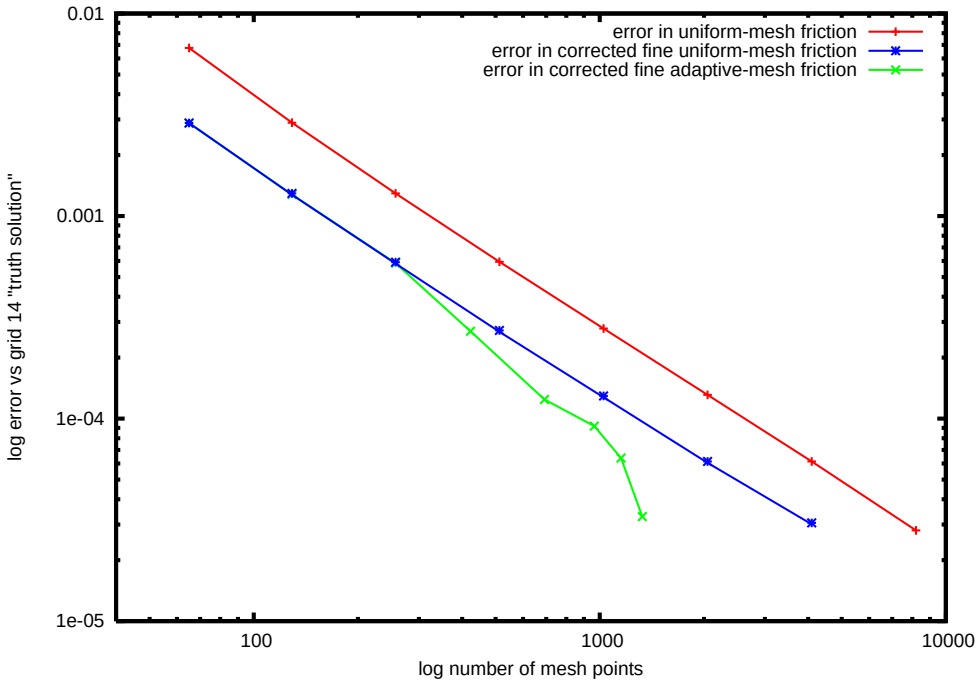

Figure 6. Comparison of predicted fine-grid errors in the friction compared against a grid 14 "truth" solution.

Figure 6 shows the substantially improved efficiency of using, appropriately driven, local refinement.

In Figure 7 the level of mesh refinement, for this example, is shown throughout the domain. This verifies that the first few levels of refinement are indeed global, before local refinement is seen to occur. This is heaviest in the region around the pressure spike but is also significant near to the entry of the contact, where the pressure first begins to grow significantly. There is also heavy refinement right up against the free boundary due to the sensitivity of the friction to the position X_c. Also included on this graph is the refinement pattern that occurs when the residual is used to drive mesh refinement. This results in much greater refinement away from the contact region (where the pressure is almost constant, as shown in Figure 4, hence contributing very little to the friction), leading to a much larger number of unknowns than arises from the adjoint-based method even though the resulting friction calculations are almost identical.

5. Conclusions and future work

In this work goal-based *a posteriori* error estimates, based upon the techniques of Darmofal and Venditti [18–20], have been developed for, and applied to, the EHL line contact problem. The property of primary interest when solving EHL problems is typically the total friction through the contact, and so this has been used as the goal in this presentation. The extension to other quantities of interest is straightforward however and is demonstrated for a variety of functionals in [9].

To the authors' knowledge this is the first example of the successful application of the adjoint-based

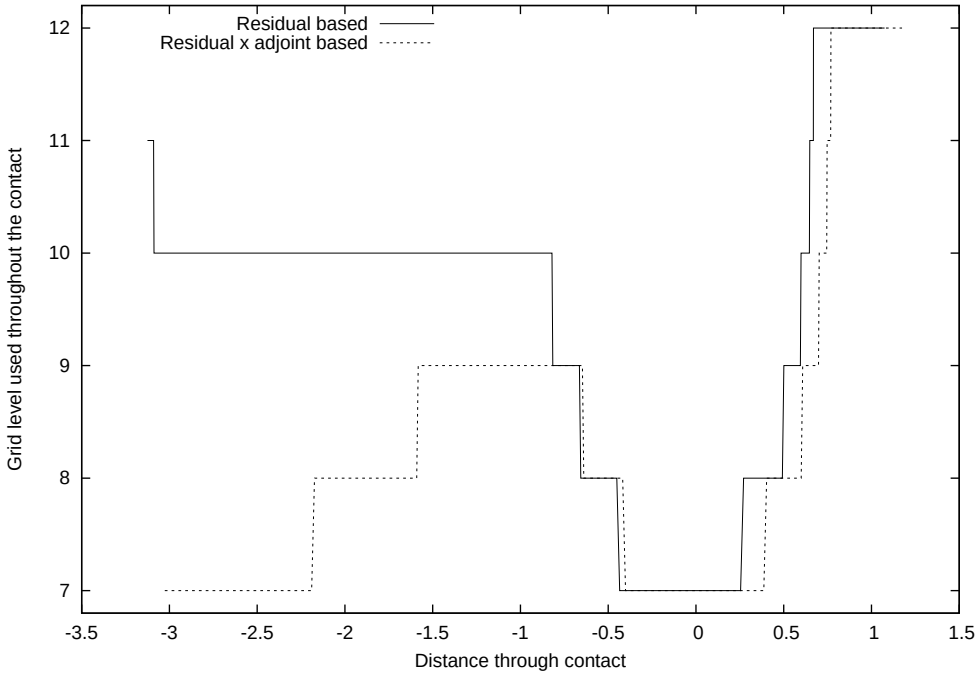

Figure 7. Local refinement levels shown for the adaptive solution of an EHL case ($L = 120000$), with refinement based on either the residual alone or the product of the adjoint solution and the residual.

error estimation approach for EHL problems. The quality of the resulting error estimate is clearly demonstrated for a variety of configurations, which range from almost purely hydrodynamic contacts through to very highly loaded EHL cases. Even on relatively coarse meshes the correction terms are remarkably accurate and, as the mesh becomes finer, the effectivity ratio is clearly seen to tend to one in all cases considered. The extension of the use of the error estimate in order to control local mesh refinement is also considered, and shown to yield improved computational efficiency alongside the reliable error estimates.

Having demonstrated the feasibility of this approach for EHL problems the way is now open to exploit this across a wider range of applications. Perhaps the most obvious extension to consider is to apply the technique to more complex contact geometries, such as circular or elliptic point contacts for example. This would require the introduction of a second independent variable and would also need a reformulation of the free boundary problem: which would now involve an unknown curve (satisfying $\frac{\partial P}{\partial n} = 0$) rather than an unknown point X_c (where $\frac{dP}{dX} = 0$). A possible approach to resolving this would be to consider using a penalty method [13, 22] as part of the discretization. However this would have the effect of no longer representing the free boundary explicitly as part of the solution and so would require the adjoint formulation to be modified accordingly.

Acknowledgements

DEH would like to thank The UK Engineering and Physical Sciences Research Council and Shell Global Solutions for their financial support during the course of this work.

REFERENCES

1. Bissett EJ, Glander DW. A highly accurate approach that resolves the pressure spike of elastohydrodynamic lubrication. *Journal of Tribology* 1988; **110** : 241–246.
2. Blau PJ. *Friction Science and Technology*. Dekker, 1996.
3. Blencoe KA, Roper GW, Williams JA. The influence of lubricant rheology and surface topography in modelling friction at concentrated contacts. *Proceedings of the Institution of Mechanical Engineers Part J, Journal of Engineering Tribology* 1998; **212(6)** : 391–400, DOI: 10.1243/1350650981542209.
4. Dowson D, Higginson GR. *Elasto-hydrodynamic Lubrication, The Fundamentals of Roller and Gear Lubrication*. Permagon Press, Oxford, Great Britain, 1966.
5. Goodyer CE, Berzins M, Jimack PK, Scales LE. Grid-based numerical optimisation in a problem solving environment. In: S. Cox (editor), *Proc. All Hands Meeting 2003* : 854–861. EPSRC, 2003. ISBN: 1-904425-11-9.
6. Goodyer CE, Berzins M, Jimack PK, Scales LE. A Grid-enabled problem solving environment for parallel computational engineering design. *Advances in Engineering Software* 2006; **37** : 439–449, DOI: 10.1016/j.advengsoft.2005.09.007.
7. Goodyer CE, Fairlie R, Hart DE, Berzins M, Scales LE. Calculation of friction in steady-state and transient EHL simulations. In: A. Lubrecht and G. Dalmaz (editors), *Transient Processes in Tribology: Proceedings of the 30th Leeds-Lyon Symposium on Tribology* 2004; 579–590. Elsevier.
8. Goodyer, CE; Wood, J; Berzins, M A parallel grid based PSE for EHL problems. In: Fagerholm, J.; Haataja, J.; Järvinen, J.; Lyly, M.; Raback, P.; Savolainen, V. (editors) Applied Parallel Computing Advanced Scientific Computing 6th Internat ional Conference, PARA 2002, pp.521-530. Springer-Verlag. 2002.
9. Hart DE. *Adjoint Error Estimation for Elastohydrodynamic Lubrication*, PhD Thesis, School of Computing, University of Leeds, 2008. Available from http://www.comp.leeds.ac.uk/research/pubs/theses/hart.pdf
10. Hart DE, Goodyer CE, Berzins M, Jimack PK, Scales LE. Adjoint error estimation for EHL-like models. *International Journal for Numerical Methods in Fluids* 2005; **47** : 1069–1075, DOI: 10.1002/fld.881.
11. Hart DE, Goodyer CE, Berzins M, Jimack PK, Scales LE. Adjoint error estimation and spatial adaptivity for EHL-like models. *IUTAM Symposium on Elastohydrodynamics And Micro-elastohydrodynamics: Proceedings of the IUTAM Symposium Held in Cardiff, UK, 1-3 September 2004* : 47–58, 2006, DOI: 10.1007/1-4020-4533-6_3.
12. Lu H, Berzins M, Goodyer, CE, Jimack PK. High order discontinuous Galerkin method for EHL line contact problems. *Communication in Numerical Methods in Engineering* 2005 **21(11)** : 643–650, DOI: 10.1002/cnm.781.
13. Lu H, Berzins M, Goodyer CE, Jimack PK, Walkley MA. Adaptive high-order finite element solutions of transient elastohydrodynamic lubrication problems. *Proceedings of the Institution of Mechanical Engineers Part J, Journal of Engineering Tribology* 2006; **220(3)** : 215–225, DOI: 10.1243/13506501JET134.
14. Nadarajah S, Jameson A. A comparison of the continuous and discrete adjoint approach to automatic aerodynamic optimization. In: *Proceedings of the 38th Aerospace Sciences Meeting and Exhibit, Reno, NV*, AIAA-200-0667. 2000.
15. Pierce NA, Giles MB. Adjoint recovery of superconvergent functionals from PDE approximations. *SIAM Review* 2000; **42(2)** : 247–264, DOI: 10.1137/S0036144598349423.
16. Roelands CJA. *Correlational Aspects of the viscosity-temperature-pressure relationship of lubricating oils*. Ph.D. Thesis, Technische Hogeschool Delft, The Netherlands, 1966.
17. Scales LE. Quantifying the rheological basis of traction fluid performance. In: *Proceedings of the SAE International Fuels and Lubricants Meeting, Toronto, Canada*. Society of Automotive Engineers, 1999.
18. Venditti DA, Darmofal DL. Adjoint error estimation and grid adaptation for functional outputs: Application to quasi-one-dimensional flow. *Journal of Computational Physics* 2000; **164** : 204–227, DOI: 10.1006/jcph.2000.6600.
19. Venditti DA, Darmofal DL. Grid adaptation for functional outputs: Application to two-dimensional inviscid flows. *Journal of Computational Physics* 2002; **176** : 40–69, DOI: 10.1006/jcph.2001.6967.
20. Venditti DA, Darmofal DL. Output-based error estimation and adaptation for aerodynamics. In: H.A. Mang and F.G. Rammerstorfer (editors), *Fifth World Congress on Computational Mechanics*. 2002.
21. Workel MF, Dowson D, Ehret P, Taylor CM. The influence of mean contact pressure on the friction coefficient of a traction fluid at high pressure. *Proceedings of the Institute of Mechanical Engineers Part C, Journal of Mechanical Engineering Science* 2000; **214(2)** : 309–312, DOI: 10.1243/0954406001522976.
22. Wu SR. A penalty formulation and numerical approximation of the Reynolds-Hertz problem of elastohydrodynamic lubrication. *International Journal of Engineering Science* 1986; **24** : 1001–1013, DOI: 10.1016/0020-7225(86)90032-7.